

# Understanding Neutrino Interactions with Liquid Argon Time Projection Chambers

Cristian Gaidau

*Department of Physics, Kansas State University, Manhattan, KS 66506*

(e-mail: cristi2206@gmail.com)

Mentors: Dr. Tim Bolton, Dr. Glenn Horton-Smith and David McKee

August 5, 2010

## Abstract

The neutrino is an elementary particle which belongs to the lepton family. Having no electric charge and a very small mass, neutrinos rarely interact with ordinary matter, which make the experimental studies difficult. MicroBooNE will be an experiment aimed at studying these elusive particles. In this paper, we devise a systematic procedure of visually analyzing the events that will be detected at MicroBooNE.

## 1. Introduction

MicroBooNE is a detector which will be built incident to the Booster Neutrino beam (BooNE). The active volume of the detector consists of 100 tons of liquid argon. It will employ the Liquid Argon Time Projection Chamber (LAr TPC) technique, which will allow high resolution of the events. In this respect, MicroBooNE is a successor of the smaller ArgoNeuT experiment and is an intermediate step towards large scale LAr TPC detectors. The container will be encircled by three planes of wires that will detect the ionization produced by the particles travelling through the liquid argon.

The primary goal of the MicroBooNE experiment is to study the low energy neutrino interactions and to investigate the unexplained excess of low energy electron neutrino events detected by the MiniBooNE experiment. As mentioned above, LAr TPC produces high resolution images of the tracks – comparable to the resolution of bubble chambers – and having three detector planes will allow a full reconstruction of the detected events. However, LAr TPC is a relatively new technique in particle physics and, as of yet, there is no automated software for analyzing this data. This paper presents an algorithmic procedure developed for human hand-scanning, which will be used to test the performance of the software.

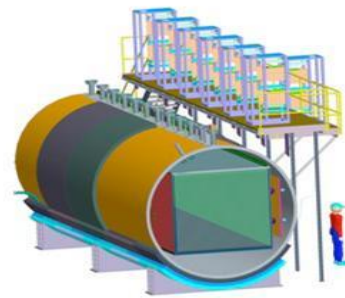


Fig.1 The MicroBooNE detector

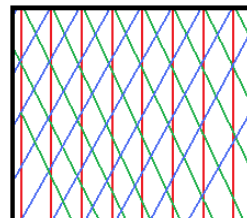


Fig.2 The arrangement of the detector planes:  
Red lines – Collection Plane  
Blue and green lines – 1<sup>st</sup> and 2<sup>nd</sup> Induction Planes

## 2. Background Information

MicroBooNE will study the neutrinos from the Booster neutrino beam. The Booster beam consists of muon and electron neutrinos. However, as Figure 3 shows, electron neutrinos make up only a tiny fraction ( $\sim 1\%$ ) of the total flux.

The three classes of neutrino interactions that will occur in the detector are: charged current electron neutrino (CC  $\nu_e$ ), charged current muon neutrino (CC  $\nu_\mu$ ) and neutral current (NC). MicroBooNE will primarily investigate the CC  $\nu_e$  events, but given the tiny percentage of  $\nu_e$  in the beam, the rate of these interactions will be very small compared to the total. This circumstance has important implications in the structure of the algorithm, because it will have to accomplish two tasks simultaneously:

- 1.) to reject a large fraction of the events in a small number of steps.
- 2.) to have a low tolerance for both false positive and false negative CC  $\nu_e$  events.

Task two is especially important because the fraction of misidentifications has to be much smaller than the set of CC  $\nu_e$  events, which itself will be minuscule compared to the other interaction channels.

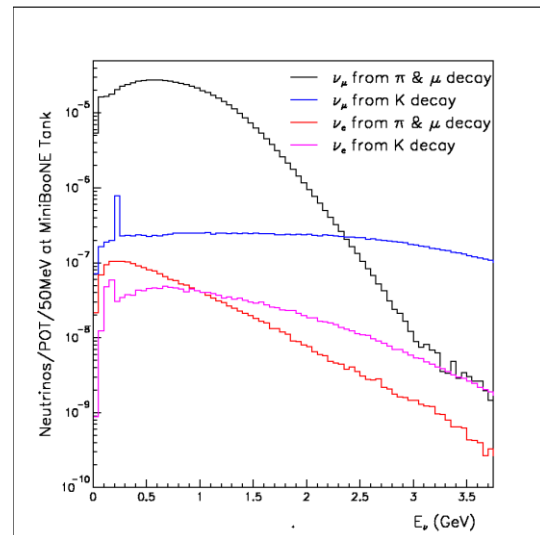


Figure 3. “Neutrino flux, for different neutrino parentage vs true neutrino energy”

Picture taken from the BooNE official webpage: [http://www-boone.fnal.gov/for\\_physicists/imagesforphys/newflux.html](http://www-boone.fnal.gov/for_physicists/imagesforphys/newflux.html)

## 3. The Algorithm

### 3.1 Step 1: Well Contained Events

There is a certain set of minimal conditions that are required for the classification of an event. One of the first conditions is the ability to locate the primary vertex of interaction. Ideally, the neutrino would interact in the bulk of the active volume. However, this is not always the case. For example, the neutrino interacts with an iron nucleus of the wall of the detector. In this case, not all of the produced particles will be detected, thus, one cannot reconstruct the interaction. These are the events that are not well contained. This is the first class of events that are discarded. Figure 4 is an example of an uncontained event. On the other hand, in a well contained event the primary vertex can be determined unambiguously, the particles do not leave the detector or their identity can be established based on the contained section of the track. Figure 5 presents a well contained event. The characteristic properties of the primary vertex are:

- all primary tracks connect to the primary vertex. If there is gap, the track can be extrapolated back to the primary vertex.
- the primary vertex has the same time location in both the induction planes and the collection plane.
- there is a large energy deposition at the primary vertex. Typically it spans for 1-5 wires. Typical energy deposition range from 300 up to 2000 Analog Digital Converter (ADC) units in the collection plane.

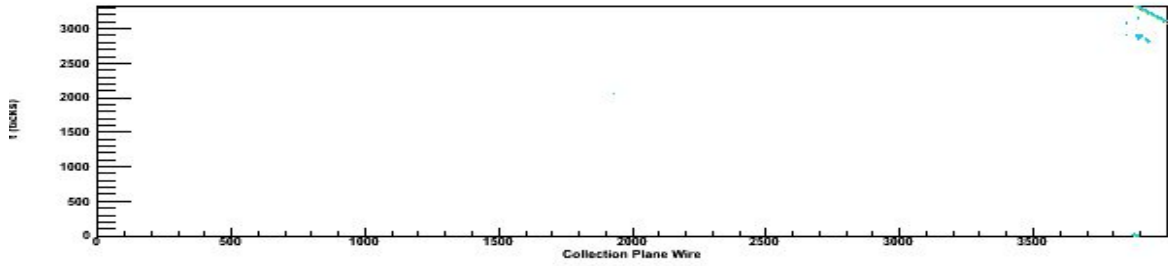


Fig.4 Example of an event that is not contained

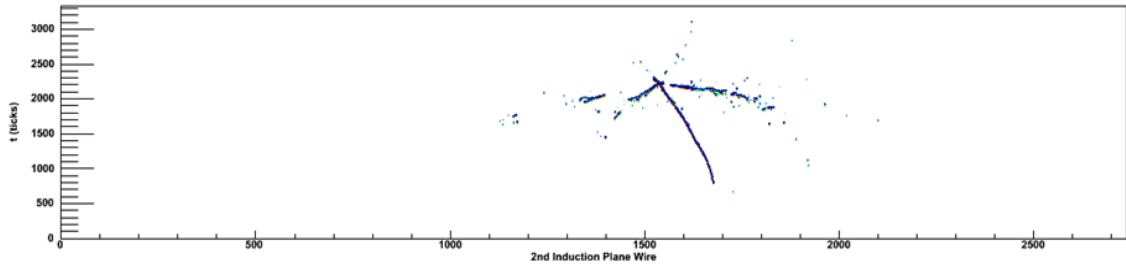


Fig. 5 A well contained event

It should be noted that there is no strict distinction between well contained events and events that are not well contained. Figure 6 provides such an example. If it is impossible to identify the particle using the subsequent steps, then the event should be discarded.

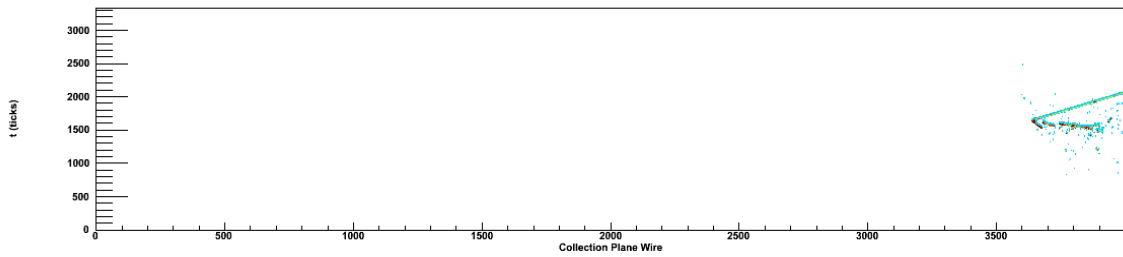


Fig.6 We can easily locate the primary vertex. However, it may not be obvious which particles were produced in the interaction. In this case, the straight track could be produced by a muon or a pion.

Also, the fact that an event is well contained does not necessarily imply that the primary vertex can be determined unambiguously. Figure 7 presents such a case.

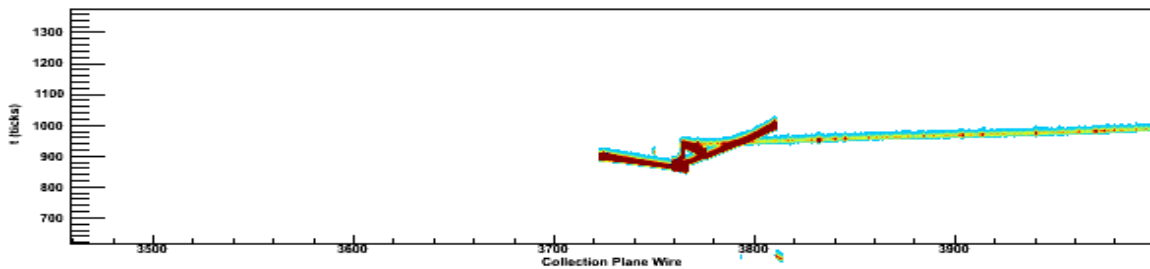


Fig.7 The event is well contained. However, the location of the primary vertex is unclear.

For human hand-scanning, the solution of this problem is to have the actual 3D reconstruction of the event. In that view the primary vertex is the one which occurs earlier in time.

Before we move on to the next step, we should take into consideration the following facts: in CC  $\nu_e$  interactions an electron is produced at the primary vertex; in CC  $\nu_\mu$  interactions a muon is

produced at the primary vertex; in NC interactions neither electrons nor muons are created at the primary vertex. These facts constitute the outline of the subsequent steps.

### 3.2 Step 2: Events which contain shower(s)

One primary characteristic of the electron is that it produces an electromagnetic shower in the detector. Visually, an electromagnetic shower is described as a region of high concentration of isolated spots of energy deposition which, taken as a connected region, resembles the geometry of a cone i.e. the shower “spreads”. Figure 8 shows a shower example.

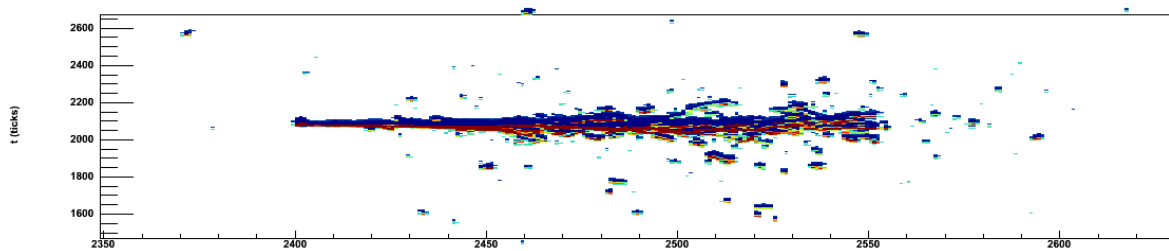


Fig.8 A typical electromagnetic shower. Notice the “branching” and “forking” of the shower.

If the event does not contain a shower it is guaranteed that this is not a CC  $\nu_e$  interaction, therefore we reject this event. The reason is that in any identifiable CC  $\nu_e$  interaction there will be at least one electromagnetic shower, which was caused by the electron. Note that at this point we do not attempt to identify the particle which caused the shower. At this point we reject all NC quasi-elastic (QE) and CC QE  $\nu_\mu$  events, because neither of the two classes of interactions involve the production of showering particles, namely: electrons, photons, pions and kaons.

### 3.3 Step 3: $\mu$ Identification

The characteristic properties of a  $\mu$  track are:

- a long straight track, typically spanning over 700 wires, connecting to the primary vertex
- minimum ionizing. The energy deposition range is from 10 up to 50 ADC units, with the average ionization being 30-35 ADC units.
- in approximately 2/3 of the CC  $\nu_\mu$  events the muon will leave the detector regardless of location of the primary vertex. If the muon does not leave the volume of the detector, the track will be characteristic of a particle that stops and decays: increasing energy deposition along the track, with a high energy deposition at the end of the track, followed by a low energy electromagnetic shower caused by decay products (electron or positron, depending on the charge of the muon).

Minor changes in the characteristics of the track start to occur, as the energy of the muon increases. These differences are illustrated in Figure 9. If a muon is successfully identified, the event can be rejected because it belongs to the CC  $\nu_\mu$  class.

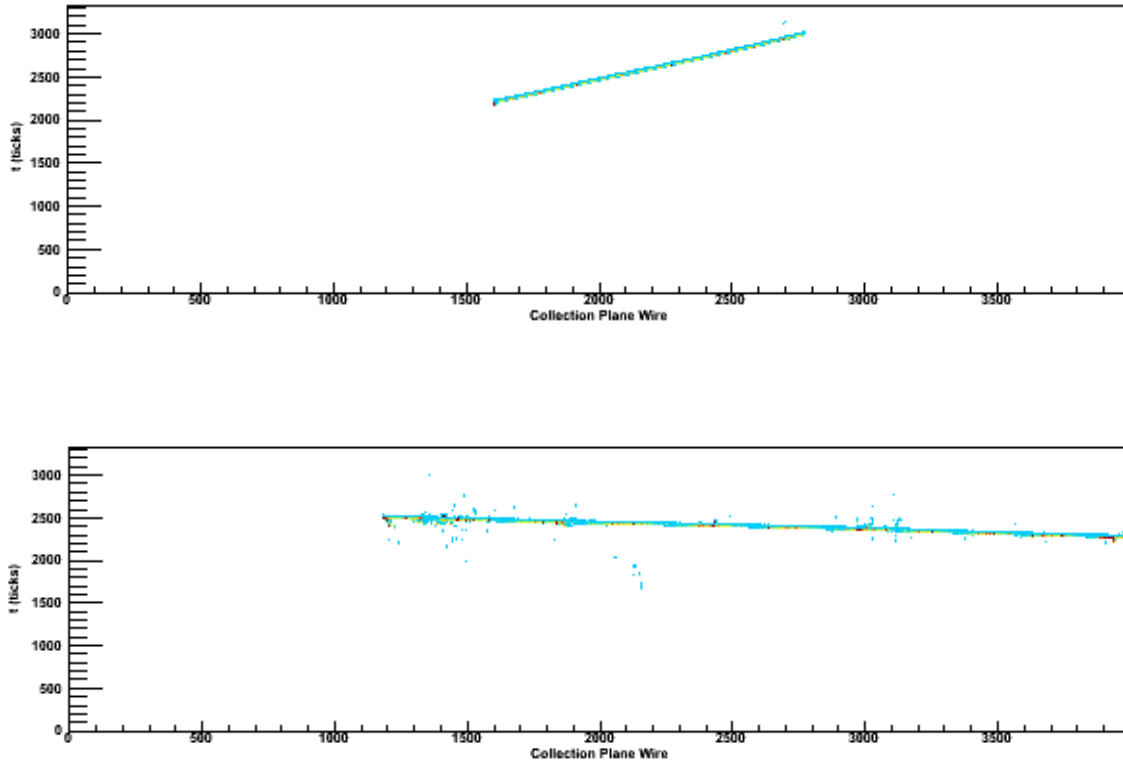


Fig. 9 The upper picture presents the track of a 1.85 GeV muon. This track is characteristic for muon energies up to 2 GeV, this was the predominant range of muon energies in the events that were hand-scanned. The picture just above shows the track of a 18.40 GeV muon. This track is typical for muon energies larger than 2 GeV, however such events were much more rare. Notice the slight difference: the track of the 1.85 GeV muons is “clean”, whereas the 18.40 GeV muon produces substantial ionization in the proximity of the track.

### 3.4 Step 4: Identification of the showering particle

In this step we need to separate the CC  $\nu_e$  events from the NC RES and NC DIS events. The primary particles that are commonly produced in the neutral current resonant and deep inelastic scattering modes are: protons, neutrons, charged pions, neutral pions and photons.

The nucleons (protons and neutrons) are not of particular interest in this algorithm for two main reasons:

- 1.) The neutrons have no electric charge, therefore they will not leave an ionizing track in the detector.
- 2.) The protons are typically produced with an energy in the 0.94 GeV – 2.00 GeV range. The proton track is straight and highly ionizing, with energy deposition of 80 to 100 ADC units. Having a small momentum, the proton track does not extend for more than 100 wires, and exhibits the characteristic properties of a stopping particle, with an energy deposition at the end of the track being in the interval 200 – 300 ADC units. Therefore, it is relatively easy to differentiate between protons and muons.

On the other hand, the pions and the photons do produce showers and, for that reason, require a more careful description.

#### 3.4.1 The description of $\pi^\pm$ tracks

The charged pions will typically decay within the active volume of the detector. The predominant decay channel is  $\pi^+ \rightarrow \mu^+ + \nu_\mu$  and  $\pi^- \rightarrow \mu^- + \bar{\nu}_\mu$ . For energies larger than 1 GeV, a characteristic feature of a well contained pion track is that it contains one or more sharp turns. Such a kink can be explained by the fact that the pion decayed or that it had a secondary interaction with an

argon nucleus. In both cases, the initial fragment of the pion track typically spans for 100-300 wires. The energy deposition of the track varies in the interval 40 – 80 ADC units. If the event is at the edge of the fiducial volume, the pion can escape the detector without decaying or having a secondary interaction. In that case, the track will be very similar to a muon track (figure 6 for example). In that case, energy deposition can be used as a factor to differentiate the two particles. A common pion track is presented in Figure 10.

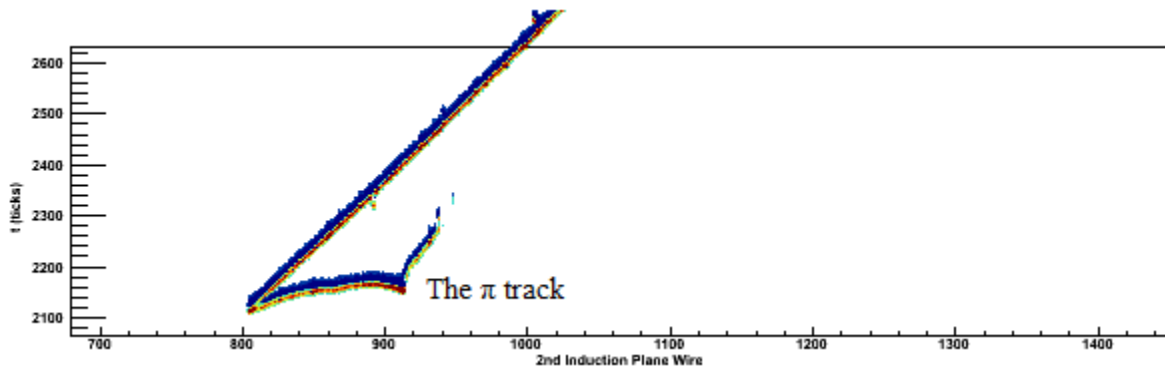


Fig. 10 A typical pion track. Notice the sharp bent in the track.

In the case of pion energies less than 1 GeV, it is likely than the pion will decay right at the vertex. Figure 11 shows an example of such a scenario.

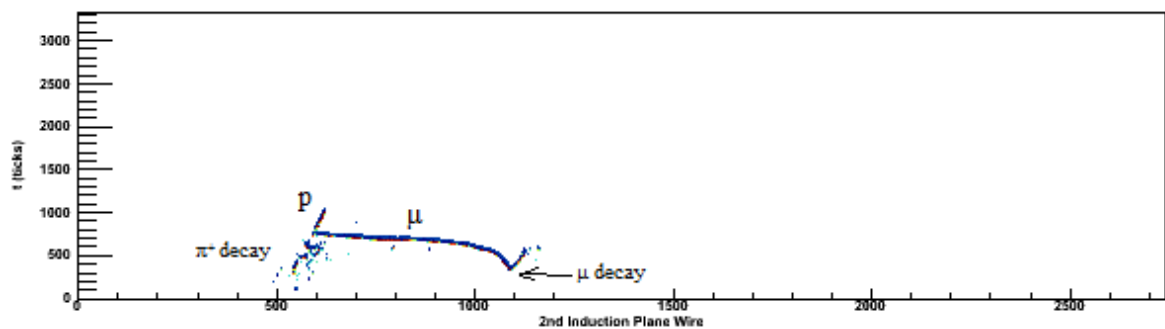


Fig. 11 The pion decay looks very similar to an electromagnetic shower. The energy of the pion is 0.30 GeV. Having a low energy, the pion quickly decays to a muon. The muon itself has a low energy, and decays to an electron, which produces the electromagnetic shower

In such cases, the primary vertex should be investigated at higher resolution, because there is typically a very short charged pion track extending for 3-5 wires.

### 3.4.2 The photon shower

The photon produces an electromagnetic shower almost immediately after being created at the primary vertex. Typically there is a small “gap” of 3-8 wires between the vertex and the start of the shower.

### 3.4.3 $\pi^0$ showers

The  $\pi^0$  has a very short lifetime ( $\sim 10^{-17}$  s) and always decays within the active volume of the detector. The predominant decay mode is  $\pi^0 \rightarrow \gamma\gamma$ . The two photons produce the characteristic electromagnetic shower. The signature of the pion is the presence of a “gap” between the primary vertex and the start of the shower. The length of the gap varies from 10 to 40 wires. For energies lower than 0.80 GeV the two photons can scatter at large angles and produce two separate electromagnetic showers, however both showers will point back to the primary vertex. If the energy of the pion is higher than  $\sim 1.00$  GeV, the two photons scatter at a smaller angle, causing the two

showers to overlap. A neutral pion shower is presented in Figure 12.

A possible reason for the discrepancy between the gap length of the photons produced by  $\pi^0$  and the photons produced at the vertex is that in the  $\pi^0 \rightarrow \gamma\gamma$  reactions each photon will have, on average, higher energy than the photons produced at the vertex – higher energy implies a longer mass attenuation length. However, this explanation is not conclusive.

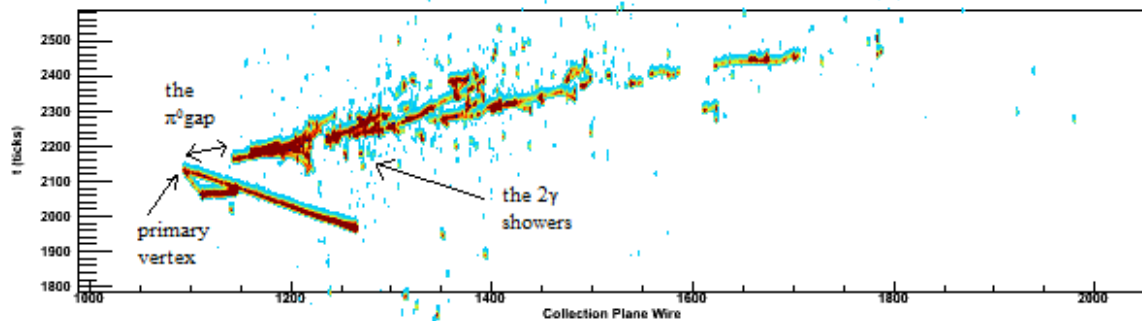


Fig. 12 A  $\pi^0$  event. The energy of the pion is 1.67 GeV

### 3.4.4 The electron shower

The properties of an electron track are:

- the electron generates an electromagnetic shower. A typical event is shown in Figure 13.
- because the electron is charged, the track must connect to the primary vertex in all three wire planes. Note that this property is crucial in differentiating electrons from photons and neutral pions.

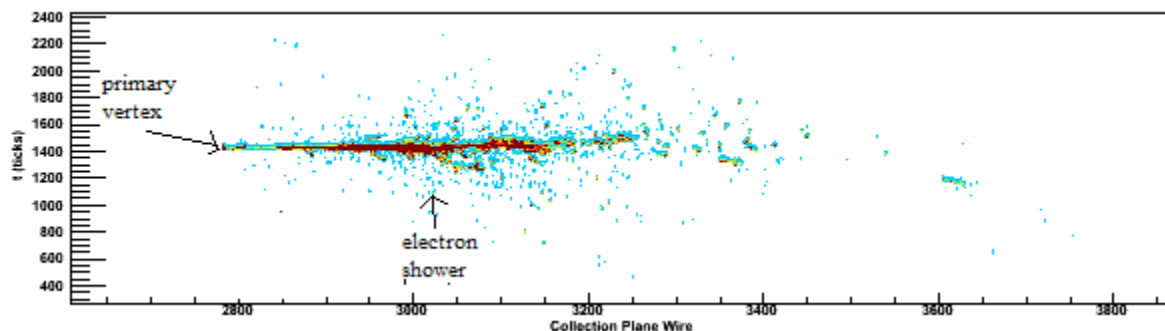


Fig 13. A typical electron shower. In this particular example, we have a CC QE  $V_e$  with the production of an electron and a proton. Although the proton track is not always visible, a high ionization at the vertex will hint that a very low energy proton was produced, which released all of it's energy within a few wires.

By comparing the photon and electron showers, we also made the following observation: the electron showers are typically more “connected”. That is, there are no gaps within the shower. On the other hand, in the photon showers there are sections of large energy deposition separated by small gaps (5 – 40 wires). Figures 12 and 13 present this difference. At this point, we have not performed a careful study of this aspect. Also, we have not investigated the energy deposition within the showers. These properties will have to be properly analyzed because they need to be taken into account when identifying the showering particle.

## 4. Efficiency tests

In order to test the efficiency algorithm we have proceeded in the following way: hand-scan a certain number of events and records the classification, and the compare the evaluation of the hand-scanned with the truth-view information. The efficiency test was performed in two steps: the preliminary test and the principal test. Both tests were performed using the LBNE simulation files. (/data/microboone/handscan/LBNE/).

In the preliminary test we have analyzed the following events:  
ccqe\_nue\_lbne.root - 30 events  
ccqe\_lbne.root - 20 events

The results of the preliminary test are: efficiency of background rejection – 100% (27/27 rejected)  
efficiency of signal retention – 100 % (23/23 accepted)

In the principal test we have analyzed the following files:  
allchannels\_lbne.root – 100 events  
ccres\_lbne.root – 30 events  
cc\_lbne.root – 30 events

The results of the principal test are:  
Note, the efficiencies were calculated as:  
number of correctly identified events/(total events + number of false positive events)

efficiency of background rejection – 96 % (154/160 rejected, NC and CC  $\nu_\mu$  combined)  
efficiency of signal retention: 7/1 accepted (i.e. 6 false positives and one correct identification)

efficiency of CC  $\nu_\mu$  identification: 93% (120/125 correctly identified)  
- 5 false negative classifications: 4 misidentified as NC and one as not contained.  
- 4 false positive events: all 4 events were NC.

efficiency of NC  $\nu$  identification: 74% (29/35 correctly identified)  
- 6 false negative: all 6 misidentified as CC  $\nu_e$   
- 4 false positive: all 4 events were CC  $\nu_\mu$

efficiency of CC  $\nu_e$  identification: 14% (1/1 correctly identified)  
- 0 false negative identifications  
- 6 false positive: all 6 were NC interactions.

efficiency of  $\pi^0$  shower identification: 68% (17/22 correctly identified)  
- 5 false negative events  
- 3 false positive events

efficiency of  $\pi^\pm$  shower identification: 70% (14/20 correctly identified)  
- 4 false negative events  
- 2 false positive events

## 5. Comments and Conclusions

All of the events that have been hand-scanned were well-contained. Thus, the efficiency of Step 1 of the algorithm could not be evaluated. In the principal test, only one CC  $\nu_e$  event was generated, for this reason, the efficiency of CC  $\nu_e$  identification cannot be evaluated. That being said, this sector needs substantial improvement in rejecting the NC events. This reinforces the importance of task 2 of this algorithm: despite the satisfactory performance of the algorithm in the NC sector, the errors induced into the CC  $\nu_e$  sector are not tolerable. The procedure also had a moderate success in identifying the meson showers. The highest performance was obtained in the CC  $\nu_\mu$  class of events. Besides the good rejection efficiency, the CC  $\nu_\mu$  and CC  $\nu_e$  sectors were 100% separated. That is, there were no false positives or false negatives in the CC  $\nu_e$  events caused by the CC  $\nu_\mu$  interactions, and vice-versa.



## 6. Future Work

At this point, the algorithm requires a more thorough efficiency assessment. This can be achieved by hand-scanning a larger data set. However, the simulations will have to employ the entire volume of the detector. This course of actions will accomplish the following: evaluate the filtering performance of the first step of the algorithm and accumulate a sufficient number of CC  $\nu_e$  events, which will allow a critical evaluation of the signal retention procedure.

In a small fraction of electron events, a small gap ( $\sim 3$  wires) between the primary vertex and the beginning of the shower has been observed. The cause of this gap is currently unknown. This topic will have to be addressed in the context of the dependence of the gap length as a function of energy of the showering particle, which was briefly mentioned in the last paragraph of section 3.4.3. Finally, the study of charged kaons, neutral kaons,  $\Sigma$  baryons and  $\Lambda$  baryons is relevant to the hand-scanning procedure, because these particles have been observed at a rate comparable to that of photon generation at the primary vertex.

## 7. Acknowledgements

I would like to thank Dr. Tim Bolton, Dr. Glenn Horton-Smith and David McKee for their guidance and support throughout the project. Thanks to Dr. Larry Weaver for the good advices and interesting talks. Also, I am grateful to Dr. Kristan Corwin for her contribution to making this summer project a pleasant experience. In addition, I would like to thank Mikhail Makouski for the valuable comments and suggestions.